Ī element present in phase II is different than the location of the Ī element in phase I), so the transition cannot be second order.

The entropy change per IPA cation, 4.5 cal/(mol deg), is 18% larger than the increase in entropy observed during the phase transition in $IPACuCl_3$ and $IPACuBr_3$.[5,6] In the later cases, this increase was associated with the onset of a simple twofold disorder. However, the copper halide lattice takes on a more compact form during that process, the observed entropy should be slightly less than that anticipated for only disorder of the anions. In $(IPA)_2CuCl_4$, on the other hand, the copper halide lattice becomes less orderly. Hence, the 18% difference in ΔS_{th} value seems quite reasonable and in accord with the structural characteristics of the transition.

Supplementary Material Available: A listing of observed and calculated structure factor amplitudes for $[(CH_3)_2CHNH_3]_2CuCl_2$ (2 pages). Ordering information is given on any current masthead page.

Thermochromism in Copper Halide Salts. 3. Isopropylammonium Tribromocuprate(II)

Darrel R. Bloomquist* and Roger D. Willett

Contribution from the Department of Chemistry, Washington State University, Pullman, Washington 99164. *Received July 21, 1981*

Abstract: Isopropylammonium tribromocuprate(II), $(CH_3)_2CHNH_3CuBr_3$, undergoes two structural transitions above room temperature. The room-temperature phase (phase III), containing linear chains of $Cu_2Br_6^{2-}$ dimers, is isomorphous with the corresponding chloride salt. The triclinic bromide salt, $P\bar{1}$, a = 12.135 (6) Å, b = 8.199 (4) Å, c = 6.397 (3) Å, α = 78.79 (3)°, β = 124.72 (2)°, γ = 117.22 (3)°, was refined to a final R value of 0.054. The intermediate phase (phase II) appears to be isomorphous with the linear chain structure of the high-temperature phase of the chloride salt. The structure of phase I is unknown. The ^1H NMR second moment decreases by 30% at the first phase transition and an additional 20% at the second phase transition. The first transition corresponds to a dynamic twofold disorder of the IPA cations in phase II; additional motion exists in phase I. The magnetic susceptibility of phase III is consistent with the observed dimeric structure, with a ground-state singlet approximately 190 K below the excited triplet state. The susceptibility of quenched phase II shows the expected strong ferromagnetic intrachain interactions. In quenched phase I, the salt shows predominant antiferromagnetic interaction, with the a transition to a weak ferromagnetic ordered state at 6 K. This indicates that the linear chain structure in phase II does not persist into phase I. Instead, a monobridged chain of $CuBr_4^{2-}$ tetrahedra is postulated for phase I.

Copper halides salts exhibit a wide variety of structural geometries, including distorted tetrahedral geometry as in Cs_2CuCl_4,[1] square pyramidal in $(C_6H_{11}NH_3)CuCl_3$,[2] squares bipyramidal in $(RNH_3)_2CuCl_4$ salts,[3] square planar in $(C_6H_5CH_2CH_2NH_2CH_3)_2CuCl_4$,[4] and trigonal bipyramidal in $Co(NH_3)_6CuCl_5$.[5] In addition, linkage isomerization leads to an incredibly wide array of structural geometries, even with a single counterion, as exhibited by the sequence $[(CH_3)_3NH]_2Cu_4Cl_{10}$,[6] $[(CH_3)_3NH]_3Cu_2Cl_7$,[7] $[(CH_3)_3NH]_2CuCl_4$, and $[(CH_3)_3NH]_3CuCl_5$.[8] The relatively comparable energies of these geometries is demonstrated by the observation of several geometries in a single salt such as distorted tetrahedral and square-bipyramidal ions in $[(CH_3)_3NH]_3Cu_2Cl_7$,[9] three distorted tetrahedral ions in $[(CH_3)_2CHNH_3]_2CuCl_4$,[10] and distorted tetrahedral, square pyramidal, and square bipyramidal in $(N(2amet)pipzh_3)_4Cu_5Cl_{22}$ where $N(2amet)pipzH_3$ is the N-2-ammoniummethylpiperazinium cation.[11] The ease of interconversion between these geometries is testified to by the phenomenon of thermochromism, where the salts undergo first-order structural phase transitions involving a change in coordination geometry.[4,12-14] Spectroscopic studies indicate that these generally involve a transformation toward tetrahedral geometries in the high-temperature phase. It is postulated that the low-temperature structure is stabilized by cation–halide hydrogen-bonding interactions. This is weakened by the onset of dynamic disorder in the high-temperature phase, allowing the electrostatic repulsion to force the complex to distort toward a tetrahedral geometry.

An exception to this trend is found in $(CH_3)_2CHNH_3CuCl_3$, abbreviated $IPACuCl_3$, in which the low-temperature phase contains an asymmetrically bibridged linear chain of symmetrically bridged dimers and the high-temperature phase contains a tribridged chain.[15] The coordination geometry changes from square pyramidal to square bipyramidal. Thus the coordination number *increases* from 5 to 6 as the temperature is raised. In the low-temperature phase, the nonbridging chloride ions of the dimer are involved in strong N–H···Cl hydrogen bonds. This is weakened by the onset of a dynamic twofold disorder of the IPA ions above the phase transition temperature. These chloride ions then find it preferable to participate in asymmetrical bridges to adjacent

* To whom correspondence should be addressed at Hewlett-Packard, Disc Memory Division, Boise, Idaho 83707.

(1) L. Helmbolz and R. F. Kruh, *J. Am. Chem. Soc.* **74**, 1176 (1952).
(2) R. Gaura, C. P. Landee, R. D. Willett, H. Groenendijk, and A. J. van Duyneveldt, *Physica A (Amsterdam)*, submitted for publication. L. Antolini, G. Marcotrigiano, L. Menabue, and G. C. Tellacani, *J. Am. Chem. Soc.*, **102**, 1303, (1980).
(3) J. P. Steadman and R. D. Willett, *Inorg. Chim. Acta*, **4**, 367 (1970).
(4) R. L. Harlow, W. J. Wells III, G. W. Watt, and S. H. Simonsen, *Inorg. Chem.*, **13**, 2106 (1974).
(5) K. N. Raymond, D. W. Meek, and J. A. Ibers, *Inorg. Chem.*, **7**, 1111 (1968).
(6) R. E. Caputo, M. J. Vukosavich, and R. D. Willett, *Acta Crystallogr., Sect. B*, **B32**, 2516 (1976).
(7) R. M. Clay, P. Murray-Rust, and J. Murray-Rust, *J. Chem. Soc., Dalton Trans.*, 595 (1973).
(8) H. Remy, and R. Laves, *Ber. Dtsch. Chem. Ges. A*, **66**, 401 (1933).
(9) R. L. Harlow and S. H. Simonsen, ACA Abstracts.
(10) D. N. Anderson and R. D. Willett, *Inorg. Chim. Acta*, **8**, 167 (1974).
(11) G. C. Pellacani, to be submitted for publication.
(12) R. D. Willett, J. A. Haugen, J. Lebsach, and J. Morrey, *Inorg. Chem.*, **13**, 2510 (1974).
(13) R. D. Willett, J. R. Ferraro, and M. Choca, *Inorg. Chem.*, **13**, 2919 (1974).
(14) G. Marcotrigiano, L. Menabue, and G. C. Pellacani, *Inorg. Chem.*, **15**, 2333 (1976).
(15) S. A. Roberts, D. R. Bloomquist, R. D. Willett and H. W. Dodgen, *J. Am. Chem. Soc.*, submitted for publication.

0002-7863/81/1503-2615$01.25/0

Table I. Compounds with Phase Transitions

compd	color	T_{trans}, °C	ΔH_{trans}, kcal/mol	ΔS_{trans}, cal/(mol deg)	T_{melt}, °C	ΔH_{melt}, kcal/mol
$IPACuCl_3$	brown-orange	85 ± 2	1.4 ± 0.2	3.9 ± 0.6	180 ± 5	6.5 ± 0.2
$IPACuBr_3$	black	78 ± 2	1.3 ± 0.2	3.7 ± 0.6		
		100 ± 2	0.8 ± 0.2	2.1 ± 0.5	143 ± 2	5.0 ± 0.3

Table II. Final Positional and Thermal Parameters for $IPACuBr_3$ Phase III (20 °C)

atom	x	y	z	U(1,1)	U(2,2)	U(3,3)	U(1,2)	U(1,3)	U(2,3)
Cu	0.5671 (2)	0.6112 (2)	0.7934 (2)	0.042 (1)	0.0288 (9)	0.0302 (9)	0.0191 (6)	0.0216 (7)	0.0135 (5)
Br(1)	0.4402 (2)	0.6557 (2)	0.3356 (2)	0.065 (1)	0.0371 (9)	0.0335 (9)	0.0327 (6)	0.0282 (7)	0.0150 (5)
Br(2)	0.6434 (1)	0.9288 (1)	0.8948 (2)	0.046 (1)	0.0276 (8)	0.0368 (9)	0.0166 (5)	0.0238 (7)	0.0080 (4)
Br(3)	0.7033 (1)	0.5547 (1)	0.2359 (2)	0.0370 (9)	0.0357 (9)	0.0318 (9)	0.0172 (5)	0.0180 (6)	0.0121 (4)
N	0.712 (1)	0.129 (2)	0.414 (2)	0.036 (6)	0.053 (7)	0.046 (6)	0.021 (5)	0.022 (5)	0.009 (5)
C(1)	0.119 (1)	0.807 (2)	0.427 (2)	0.028 (6)	0.053 (7)	0.042 (7)	0.012 (5)	0.021 (5)	0.003 (5)
C(2)	0.092 (2)	−0.025 (2)	0.352 (3)	0.051 (9)	0.08 (1)	0.052 (9)	0.044 (8)	0.017 (7)	0.007 (7)
C(3)	0.048 (2)	0.674 (2)	0.212 (3)	0.047 (9)	0.065 (9)	0.057 (9)	0.022 (7)	0.025 (8)	−0.001 (7)

atom[a]	x	y	z	atom[a]	x	y	z
N-H1	0.69 (2)	0.19 (2)	0.38 (3)	C2-H6	0.12 (2)	0.01 (2)	0.24 (3)
N-H2	0.65 (2)	−0.00 (2)	0.29 (3)	C2-H7	−0.00 (2)	0.95 (2)	0.28 (3)
N-H3	0.68 (2)	0.11 (2)	0.55 (3)	C3-H8	0.07 (2)	0.71 (2)	0.07 (3)
C1-H4	0.07 (2)	0.79 (2)	0.48 (3)	C3-H9	0.09 (2)	0.62 (2)	0.23 (3)
C2-H5	0.13 (2)	0.07 (2)	0.47 (3)	C3-H10	0.95 (2)	0.66 (2)	0.11 (3)

[a] $U = 0.0760$ Å^2.

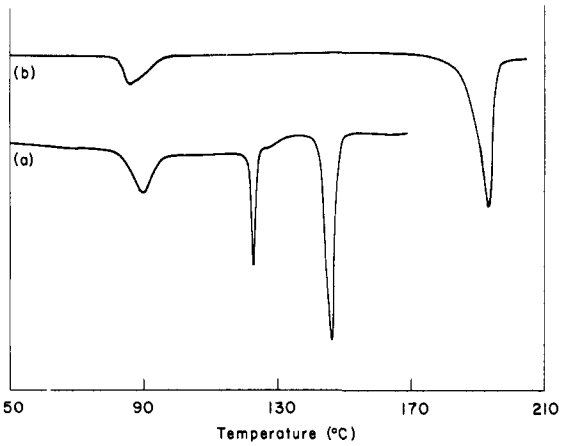

Figure 1. DTA scans for (a) $IPACuBr_3$ and (b) $IPACuCl_3$.

copper ions, thus satisfying electrostatic requirements.

Because of the uniqueness of this salt and the paucity of information on structures and structural phase transitions in copper(II) bromide salts, a study of the $IPACuBr_3$ system was undertaken.

Experimental

Crystals of $IPACuBr_3$ were separated by the same method described by Remy and Laves for $IPACuCl_3$.[8] Stoichiometric amounts of IPABr and $CuBr_2$ were dissolved in absolute alcohol and allowed to crystallize by slow evaporation. Photoreduction and/or thermal reduction of Cu(II) to Cu(I) was a problem, as is normally the case with copper(II) bromide salts. This was evidenced by the presence of a white precipitate upon redissolving any solution which was allowed to evaporate to dryness.

DTA scans, performed on a Du Pont 900 thermal analyzer, showed the existence of *two* solid-phase transitions in addition to the melting transition (Figure 1a). This is in contrast to $IPACuCl_3$ (shown in Figure 1b for comparison) in which only one solid-state transition is observed. The transition temperatures, as measured by the first deviations from base line, are 78 and 120 °C, with T_m = 145 °C. Our experience is that the solid superheats 20–30 °C, so the actual transition temperatures are substantially lower. Thermodynamic properties obtained from DSC measurements are reported in Table I.

A single crystal of $IPACuBr_3$ with dimensions 0.2 mm × 0.2 mm × 0.3 mm was mounted to rotate about its needle axis. Lattice constants for the triclinic crystals, determined from 12 accurately centered reflections (λ(Mo Kα) = 0.71069) are a = 12.135 (6) Å, b = 8.199 (4) Å, c = 6.397 (3) Å, α = 78.79 (3)°, β = 124.72 (2)°, and γ = 117.22 (3)° (Z = 2). A total of 1633 reflections were collected in the range 4° ≤ 2θ ≤ 50° on an automated Picker four-circle diffracrometer using

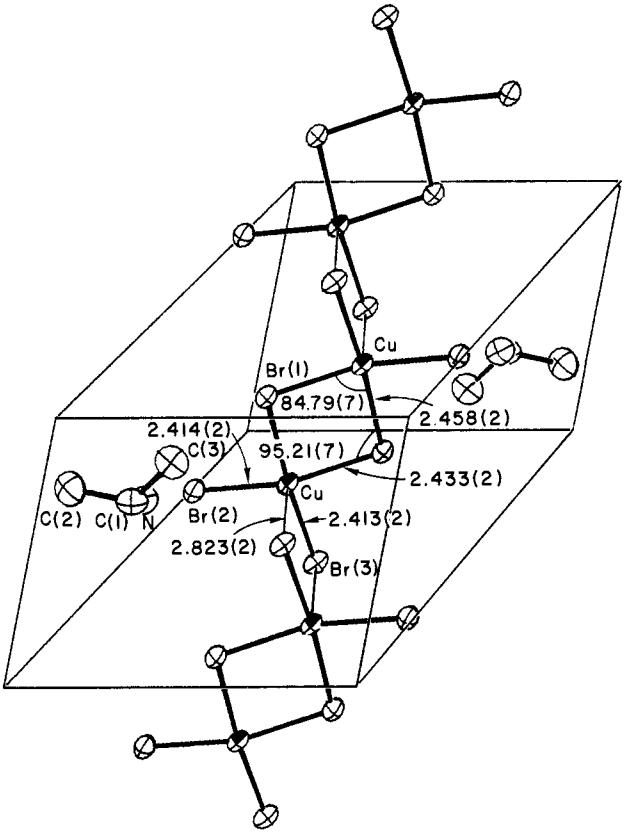

Figure 2. Unit cell of phase III (room temperature) of $IPACuBr_3$ viewed normal to bc plane.

Zr-filtered Mo Kα radiation (λ = 0.71069 Å). The data were recorded by using a 1.8° θ–2θ step scan with a step size of 0.05° and 3 s/step counting time. Background was measured for 15 s before and after each peak. The standard deviation of each reflection was calculated as $\sigma^2(I) = TC + BG + (0.03I)^2$ where TC = total counts, BG = background counts, and I = net intensity (TC − BG). The intensities of three standard reflections were monitored every 41 reflections. All data were corrected for absorption (μ = 166.7 cm^{-1}) and linear decay.

Least-squares refinement converged rapidly with all initial positions taken from the isomorphous $IPACuCl_3$ structure. Refinement of all parameters except hydrogen thermal parameters, which were fixed at 6.0, resulted in final residuals for all reflections of R = 0.074 and R_w = 0.076 with R defined as $\sum(|F_o| - |F_c|)/\sum|F_o|$ and R_w as $(\sum w(F_o - F_c)^2/$

Table III. Comparison of Bond Distances (Å) and Angles (Deg) in a Dimer System of $IPACuCl_3$ and $IPACuBr_3$ (Room-Temperature Phases)

$IPACuCl_3$		$IPACuBr_3$	
atoms	distance	atoms	distance
Cu-Cl(1)	2.301 (2)	Cu-Br(1)	2.433 (2)
Cu-Cl(1)	2.315 (1)	Cu-Br(1)	2.458 (2)
Cu-Cl(2)	2.273 (2)	Cu-Br(2)	2.414 (2)
Cu-Cl(3)	2.269 (1)	Cu-Br(3)	2.413 (2)
Cu-Cl(3)	2.699 (2)	Cu-Br(3)	2.822 (2)
Cu-Cu[a]	3.417 (1)	Cu-Cu[a]	3.613 (3)
Cu-Cu[b]	3.506 (2)	Cu-Cu[b]	3.644 (3)
$IPACuCl_3$		$IPACuBr_3$	
atoms	angle	atoms	angle
Cl(1)-Cu-Cl(1)	84.79 (6)	Br(1)-Cu-Br(1)	84.79 (7)
Cl(1)-Cu-Cl(2)	90.60 (6)	Br(1)-Cu-Br(2)	90.79 (7)
Cl(1)-Cu-Cl(2)	160.53 (8)	Br(1)-Cu-Br(2)	159.75 (8)
Cl(1)-Cu-Cl(3)	175.10 (9)	Br(1)-Cu-Br(3)	174.42 (8)
Cl(1)-Cu-Cl(3)	90.91 (6)	Br(1)-Cu-Br(3)	90.42 (7)
Cl(1)-Cu-Cl(3)[c]	100.56 (6)	Br(1)-Cu-Br(3)[c]	99.80 (7)
Cl(1)-Cu-Cl(3)[c]	91.87 (6)	Br(1)-Cu-Br(3)[c]	91.49 (7)
Cl(2)-Cu-Cl(3)	93.19 (5)	Br(2)-Cu-Br(3)	93.35 (7)
Cl(2)-Cu-Cl(3)[c]	98.42 (7)	Br(2)-Cu-Br(3)[c]	99.93 (7)
Cl(3)-Cu-Cl(3)[c]	90.65 (5)	Br(3)-Cu-Br(3)[c]	92.14 (7)
Cu-Cl(1)-Cu	95.51 (6)	Cu-Br(1)-Cu	95.21 (7)
Cu-Cl(3)-Cu	89.35 (5)	Cu-Br(3)-Cu	87.86 (7)

[a] Intradimer bond length. [b] Interdimer length. [c] Apical Cl(3).

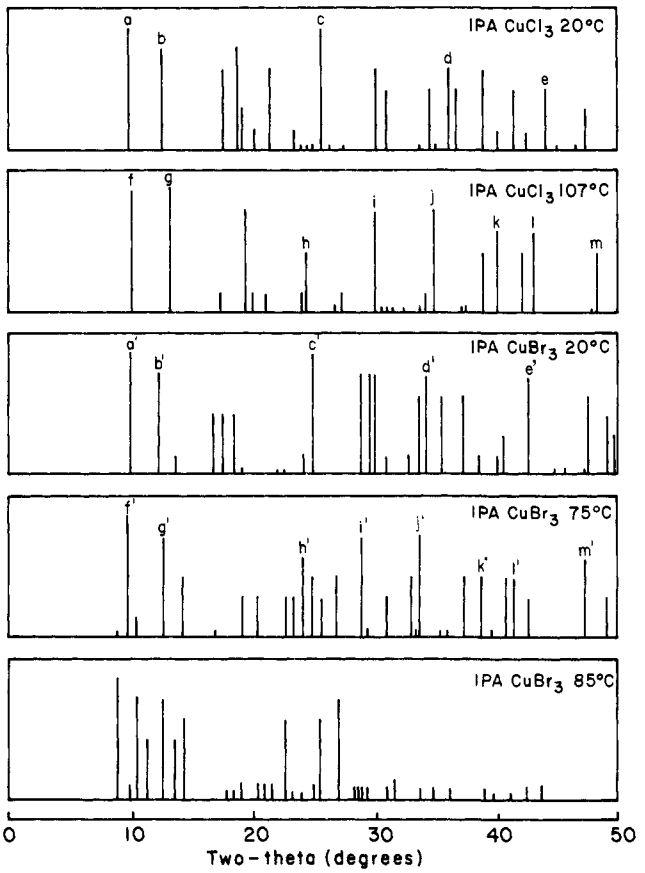

Figure 3. Powder patterns for $IPACuCl_3$ and $IPACuBr_3$ in each phase (vertical height is proportional to intensity). Equivalent maxima are lettered.

$\sum wF_o^2)^{1/2}$, where $w = 1/\sigma^2(F)$. A residual of $R = 0.054$ was achieved, omitting reflection with $F < 3\sigma$. All programs are from a local computer library.[16]

(16) D. N. Anderson, Ph.D. Thesis, Washington State University, 1971; R. E. Caputo, Ph.D. Thesis, Washington State University, 1976.

Table IV. Comparison of Bond Distances (Å) and Angles (Deg) in the IPA Cation of $IPACuCl_3$ and $IPACuBr_3$ (Room-Temperature Phase)

$IPACuCl_3$		$IPACuBr_3$	
atoms	distance	atoms	distance
C(1)-N	1.503 (8)	C(1)-N	1.53 (2)
C(1)-C(2)	1.53 (1)	C(1)-C(2)	1.49 (2)
C(1)-C(3)	1.49 (1)	C(1)-C(3)	1.48 (2)
N-NH1	0.84 (11)	N-NH1	0.63 (17)
N-NH2	0.82 (10)	N-NH2	1.12 (12)
N-NH3	1.05 (13)	N-NH3	1.05 (16)
C(1)-C1H4	1.06 (11)	C(1)-C1H4	0.76 (15)
C(2)-C2H5	1.06 (11)	C(2)-C2H5	0.94 (12)
C(2)-C2H6	0.84 (12)	C(2)-C2H6	0.91 (16)
C(2)-C2H7	1.03 (10)	C(2)-C2H7	0.90 (17)
C(3)-C3H8	1.05 (12)	C(3)-C3H8	1.07 (7)
C(3)-C3H9	0.88 (11)	C(3)-C3H9	0.77 (15)
C(3)-C3H10	1.06 (8)	C(3)-C3H10	0.93 (17)
$IPACuCl_3$		$IPACuBr_3$	
atoms	angles	atoms	angles
N-C(1)-C(2)	107.8 (5)	N-C(1)-C(2)	107.2 (11)
N-C(1)-C(3)	109.8 (7)	N-C(1)-C(3)	109.7 (12)
C(2)-C(1)-C(3)	113.8 (5)	C(2)-C(1)-C(3)	115.2 (13)
N-C(1)-C1H4	104 (4)	N-C(1)-C1H4	125 (12)
C(2)-C(1)-C1H4	108 (6)	C(2)-C(1)-C1H4	80 (13)
C(3)-C(1)-C1H4	112 (5)	C(3)-C(1)-C1H4	115 (10)
C(1)-N-NH1	112 (8)	C(1)-N-NH1	117 (16)
C(1)-N-NH2	109 (8)	C(1)-N-NH2	112 (7)
C(1)-N-NH3	112 (5)	C(1)-N-NH3	105 (9)
NH1-N-NH2	111 (9)	NH1-N-NH2	122 (18)
NH1-N-NH3	89 (11)	NH1-N-NH3	84 (17)
NH2-N-NH3	121 (8)	NH2-N-NH3	110 (11)
C(1)-C(2)-C2H5	120 (4)	C(1)-C(2)-C2H5	105 (3)
C(1)-C(2)-C2H6	105 (8)	C(1)-C(2)-C2H6	116 (3)
C(1)-C(2)-C2H7	113 (5)	C(1)-C(2)-C2H7	111 (10)
C2H5-C(2)-C2H6	118 (8)	C2H5-C(2)-C2H6	118 (14)
C2H5-C(2)-C2H7	94 (8)	C2H5-C(2)-C2H7	93 (11)
C2H6-C(2)-C2H7	105 (8)	C2H6-C(2)-C2H7	115 (15)
C(1)-C(3)-C3H8	120 (5)	C(1)-C(3)-C3H8	123 (8)
C(1)-C(3)-C3H9	117 (6)	C(1)-C(3)-C3H9	118 (12)
C(1)-C(3)-C3H10	118 (7)	C(1)-C(3)-C3H10	106 (7)
C3H8-C(3)-C3H9	92 (10)	C3H8-C(3)-C3H9	74 (14)
C3H8-C(3)-C3H10	102 (7)	C3H8-C(3)-C3H10	97 (13)
C3H9-C(3)-C3H10	101 (7)	C3H9-C(3)-C3H10	132 (14)

Final positional parameters are listed in Table II and an ORTEP drawing of the unit cell is shown in Figure 2. Tables III and IV compare bond distances and angles for the room-temperature structures of $IPACuCl_3$ and $IPACuBr_3$.

With use of a powder camera modified for variable-temperature measurements between 20 and 200 °C, diffraction patterns of the different phases of $IPACuCl_3$ and $IPACuBr_3$ were obtained, confirming the presence of a second phase transition in $IPACuBr_3$ (see Figure 3). The intermediate phase of $IPACuBr_3$ (phase II) appears to be isomorphous with the high-temperature phase of $IPACuCl_3$. Some of the diffraction maxima believed to be equivalent are lettered in Figure 3. The powder diffraction pattern of the highest temperature phase of $IPACuBr_3$ (phase I) is quite different from the other patterns, indicating an unknown structural rearrangement.

The ^1H NMR spectra were collected with a continuous-wave instrument with a phase-sensitive detection design incorporating a PAR lock-in amplifier and a Varian V-4210A variable-frequency R-F unit. Data were recorded, while sweeping the magnetic field, with a FabriTech 1052 LSH 1024 points signal averager interfaced with a Motorola microprocessor. Temperature control was maintained to within ±0.1 °C with a fluid circulation system.[17] Data were collected over the temperature range 25–104 °C.

Magnetic susceptibility data were recorded on a PAR vibrating sample magnetometer.[18] Measurements on phase III were made on a 0.2235 g sample enclosed in a gel capsule. Data for phases II and I were obtained by heating similarily encapsulated samples (0.2141 and 0.1765

(17) D. R. Bloomquist and H. W. Dodgen, to be submitted for publication.
(18) C. P. Landee, S. A. Roberts, and R. D. Willett, *J. Chem. Phys.*, **68**, 4574 (1978).

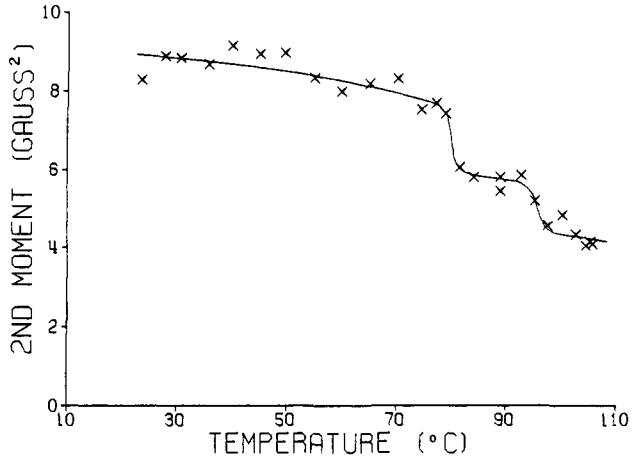

Figure 4. NMR second moment vs. temperature for $IPACuBr_3$.

g, respectively) in an oil bath set at a temperature just above the appropriate phase transition and then rapidly quenching the sample in liquid N_2. The samples were then transferred to the Janis Dewar associated with the magnetometer. Corrections for diamagnetism -144.6×10^{-6} emu/mol and temperature-independent paramagnetism 60×10^{-6} emu/mol were made.

Structural Results

The results of the single-crystal structure determination of phase III show that it is isomorphous with the room-temperature structure of $IPACuCl_3$. As seen in Figure 2, the structure consists of linear chains of symmetrically bibridged $Cu_2Br_6^{2-}$ anions. Bridging distances are 2.433 (2) and 2.458 (2) Å with a bridging angle of 95.21 (7)°. The asymmetric bridges between dimers have lengths 2.413 (2) and 2.823 (2) Å. This gives each copper ion a pronounced square-pyramidal coordination geometry. the trans Br–Cu–Br angles in the basal plane are 159.75 (8) and 174.42 (8)°. The terminal bromide which does not participate in bridge formation, Br(2), is involved in strong hydrogen bonding to the IPA ion. This provides electrostatic stability for Br(2). Tables III and IV summarize the structure information for both $IPACuCl_3$ and $IPACuBr_3$. All distances and angles compare quite closely. The Cu–Br distances are all ~0.14 Å longer than the Cu–Cl distances. The largest change in angle is the asymmetric bridging angles between dimers which is 2° smaller for the bromide salt.

The powder diffraction patterns show that phase II of $IPACuBr_3$ is isomorphous with the high-temperature phase of $IPACuCl_3$. The latter contains tribridged linear $(CuCl_3)_n^{n-}$ chains, with the IPA ions dynamically disordered about a twofold axis. The salt is orthorhombic, space group *Pcan*. Each copper ion has a square-bipyramidal coordination geometry, with one symmetrical and two asymmetrical bridges between adjacent copper ions along the chain. We conclude that phase II of $IPACuB_3$ contains this same basic structure. It is derived simply from the structure in Figure 2 by having the Br(2) ion move cooperatively into bridging positions between adjacent copper ions. The IPA ions simultaneously become disordered. The transition must be first order, since the space group of phase III ($P\bar{1}$) is not a subgroup of the phase II space group (*Pcan*). In phase III, the $\bar{1}$ element is at the center of the dimer; in phase II, the Cu atoms occupy sites of $\bar{1}$ symmetry.

The powder diffraction pattern of phase I is distinct from either phase II or III. We will postpone discussion of the possible structure of this phase until the NMR and susceptibility measurements have been discussed.

NMR Studies

Second moment data, collected as a function of temperature from room temperature to 104 °C, are plotted in Figure 4. Line shapes were essentially Gaussian in all phases. A drop in the second moment from 8.0 to 5.5 G^2 is observed at 75 °C corresponding to the first phase transition. A second drop to 4.0 G^2 occurs at 95 °C due to the second phase transition. The DTA and DSC results previously discussed show anomalies at slightly higher temperatures due to superheating in these experiments. The large scatter in the data is partly caused by the difficulty encountered in choosing integration limits for absorption lines that return to the base line slowly.

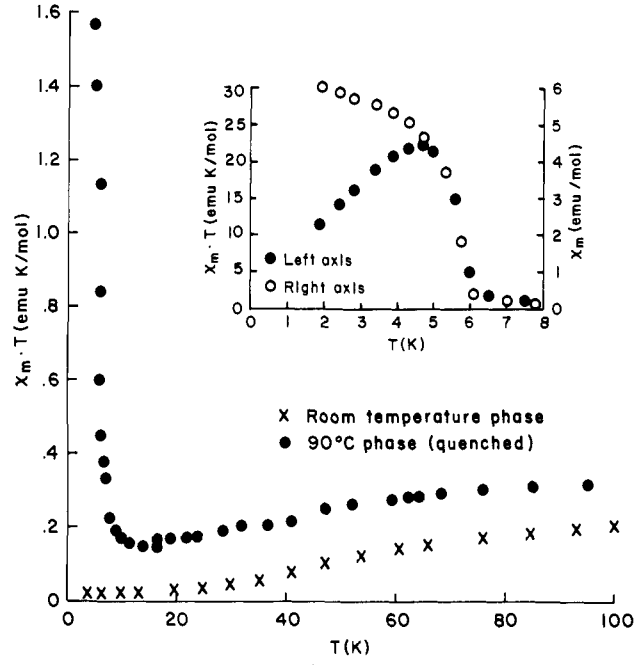

Figure 5. Magnetic susceptibility data for phase I (highest temperature) and phase III (room temperature). Insert shows temperature dependence below 8 K.

The second moment of the NMR line has been calculated for isolated IPA ions undergoing various types of disorder.[19] The absolute magnitudes cannot be compared directly to the experimental results, due to the neglect of thermal motion and intermolecular interactions. Nevertheless, the reduction in second moment seems to be an accurate diagnostic of the actual motion. These calculations predict a reduction in the second moment of 30% due to the onset of a twofold flipping of 180°. This is in precise agreement with the observed reduction for the phase III → phase II transition, in accord with the assumed disorder of the IPA cation around a twofold axis.

The total reduction of the NMR second moment for phase I is 50% (with respect to phase III). The calculations predict a 50% reduction for a disorder of the IPA cation across a mirror plane, with a flipping angle of 135°. This represents one possible type of motion for the IPA cation in phase I. Other possible models predicting a 50% reduction can be visualized.

Magnetic Susceptibility Studies

The results of the magnetic susceptibility measurements on the three phases of $IPACuBr_3$ are shown in Figure 5. Phase III shows behavior typical of and antiferromagnetically coupled system. Since χT does not extrapolate to zero, we have to assume the presence of a substantial paramagnetic impurity in the sample. This is not inconsistent with the observed ease of photodecomposition and/or thermal decomposition of copper bromide salts. Because of the structural characteristics, the susceptibility was fit to a mean field corrected Bleany–Bowers equation

$$\chi = (1 - \alpha)\frac{C}{T + \Theta}\frac{3e^{-\Delta E/kt}}{1 + 3e^{-\Delta E/kt}} + \alpha\frac{C}{T}$$

where ΔE is the singlet–triplet separation ($\Delta E > 0$, implying singlet low) for the $Cu_2Br_6^{2-}$ dimer, Θ is the mean field correction for interdimer coupling along the chain, and α is the fraction impurity (0.07). This model yield good agreement with experi-

(19) D. R. Bloomquist, R. D. Willett, and H. W. Dodgen, *J. Am. Chem. Soc.*, submitted for publication.

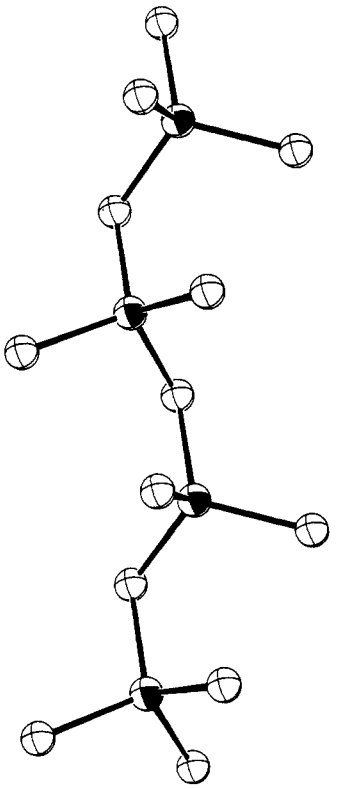

Figure 6. Proposed monobridged chain structure for phase I, $IPACuBr_3$.

ments for $\Delta E/k$ = 190 K and Θ = −20 K. This is very comparable to the results for the structurally similar system, $KCuBr_3$, where $\Delta E/k$ = 190 K and Θ = 18 K.[20] This is also consistent with the interpretation of the susceptibilty data for the room-temperature phase of $IPACuCl_3$ where the model of an Ising coupled chain of Heisenberg dimers gave $\Delta E/k = -2J_1/k$ = 46 K and $\Theta/k = 2ZJ_2/k$ = −36 K. Again the trends compare well with the pair $KCuCl_3$[21] and $KCuBr_3$, where $\Delta E/k$ = 55 and 190 K, respectively.

Finally, we note the unusual behavior of the quenched phase I. A predominant antiferromagnetic interaction is demonstrated by the gradual decrease of χT as the temperature is lowered. The high-temperature data ($T > 20$ K) show a Curie–Weiss law behavior, with Θ = 35 K (antiferromagnetic coupling). However, χT begins to increase below T = 16 K and exhibits a sharp increase at T = 6 K. This behavior is indicative of a weak ferromagnetic state. That is, there is an antisymmetric component, $\vec{d}_{jk}\vec{r}_j \times \vec{r}_k$, to the exchange coupling which leads to a canted spin structure. Two (or more) sublattices exist in which the moments are aligned nearly, but not exactly, antiparallel.

This result for the quenched phase I indicates that the copper bromide framework does not retain the tribridged $(CuBr_3)_n^{n-}$ chain structure of the intermediate phase. It does, however, provide some important clues as to the nature of the high-temperature structure. First, the dominant exchange pathway must be antiferromagnetic. Thus, any Cu–Br–Cu bridging angles must be substantially greater than 90°.[23] Second, the existence of weak ferromagnetism at low temperature means there must be an antisymmetric component to this coupling, so that the antiferromagnetic interaction cannot be associated with the presence of certain symmetry elements, e.g., a center of inversion.

Discussion

The results of this study confirm the general nature of the phase transition observed in $IPACuCl_3$. In fact, the phase III–phase II transition for $IPACuBr_3$ exactly mimics the $IPACuCl_3$ transition, and the same mechanism for the transition can be assumed. The driving force is entropic, associated with the onset of a dynamic disorder of the IPA cations. This causes an increase in the coordination number of the copper ion in phase II and a compacting of the Cu–Br framework. The latter process, by itself, would be thermodynamically unsound.

We have found, however, that the $IPACuBr_3$ system carries us one step further, to a new phase which does not exist in $IPACuCl_3$. Since the IPA ion is already disordered, the driving force must now be associated with rearrangements that occur within the Cu–Br chain. Because of the stoichiometry, a polymeric structure must necessarily be retained, most likely with a chain-type nature. It is also anticipated that the coordination number of the copper ion would decrease. The existence of a chain of dimers can reasonable be ruled out. The *intra*dimer interaction would have to be the dominant exchange interaction, and from structural characteristics, this would be antiferromagnetic. Also, a dimer would almost certainly be centrosymmetric, leading to a strictly antiparallel spin arrangement, in contradiction to the observed weak ferromagnetism. A linear chain of symmetrically bibridged copper ions, as in $(C_6H_{11}NH_3)CuCl_3$,[2] can also be ruled out since it would lead to dominant ferromagnetic coupling.

If, however, one considers the possibility of a monobridged chain, a reasonable structure can be proposed, as shown in Figure 6. Each copper assumes a distorted tetrahedral geometry. The tetrahedra share corners, with a glide-plane symmetry element relating adjacent tetrahedra. The proposed transition requires the rupture of the longest Cu–Br bonds of phase II followed by a slight twist of the tetrahedra to minimize steric repulsions between bromide ions. A Cu–Cu distance of 3.5–3.7 Å might be reasonably imagined, which would lead to a Cu–Br–Cu bridging angle of 95–100°. This could well lead to an antiferromagnetic interaction of the order observed.

In summary, $IPACuBr_3$ exhibits an interesting series of structural phase transitions, confirming the existence of only small energy differences between various stereochemical and linkage configurations. The copper ion, initially five-coordinate, is driven into a six-coordinate state by the disorder of the cation and then relaxes to a four-coordinate geometry at higher temperatures.

Supplementary Material Available: A listing of observed and calculated structure factor amplitudes for $(CH_3)_2CHNH_3CuBr_3$ (5 pages). Ordering information is given on any current masthead page.

(20) M. Inoue, M. Kishita, and M. Kubo, *Inorg. Chem.*, **6**, 900 (1967).
(21) G. Maass, B. Gerstein, and R. D. Willett, *J. Chem. Phys.*, **46**, 401 (1967).
(22) D. D. Swank, C. P. Landee, and R. D. Willett, *Phys. Rev. B: Condens. Matter*, **20**, 2154 (1979).
(23) C. Chow, R. D. Willett, and B. C. Gerstein, *Inorg. Chem.* **14**, 205 (1975).